

DANOISE; A 3D Printable Battery Cell for Laboratory Operando X-Ray Diffraction and Absorption Spectroscopy**

Morten Johansen,^[a] Jannie Kirk Verdelin,^[a] Antti-Jussi Kallio,^[b] Tommy Ole Kessler,^[a] Simo Huotari,^[b] and Dorthe Bomholdt Ravnsbæk^{*[a]}

Studying structural and electronic processes in the materials inside a battery as they occur during battery operation is key for developing novel improved materials for future generations of batteries. Such studies often entail X-ray diffraction and absorption spectroscopy, which have so far primarily been conducted at synchrotron facilities despite the widespread use of laboratory-based X-ray diffraction and absorption spectroscopy for day-to-day characterisation. With the "Developed in Aarhus: New Operando In-house Scattering Electrochemical" (DANOISE) cell, these experiments are brought into the

laboratories making in-house *operando* X-ray diffraction and absorption spectroscopy on-demand additions to the existing facilities. The chic and facile design of the DANOISE cell provides high quality scattering and absorption data besides providing reliable electrochemical performance. In this work, we describe the design of the DANOISE cell and demonstrate the capabilities of the cell using different commercial technologies for Li-ion batteries and from a new Na-ion battery electrode material.

Introduction

Rechargeable batteries, such as Li-ion batteries, are an enabling technology for the green transition. Still, the present technology needs improvements in terms of price, performance, and sustainability, and the search for new battery materials superior to the present options is ongoing.^[1]

When an ion battery is in use, the energy conversion occurs in the solid-state electrodes through oxidation and reduction accompanied by ion extraction and intercalation.^[2] These processes induce structural changes in the atomic structure of the host framework of the electrodes both due to accommodation of the active ions, e.g. Li-ions, and change in atomic radius of the species being oxidized or reduced.^[2] The structural changes can result in subtle alterations in the unit cell dimensions or in dramatic structural reconstructions with changes in the symmetry of the structure and in the atomic coordination environments. In-depth understanding of these structural changes is naturally of immense importance in the

development of novel materials as their nature determines the battery's performance and stability.^[3]

Powder X-ray diffraction (PXRD) is the go-to technique for the investigation of structural changes in poly-crystalline materials such as battery electrodes. The technique also functions very well under dynamic operating conditions, i.e., *operando* PXRD collected during battery charge and discharge is a well-established method.^[3b,4] This is a great advantage as it allows for probing the structural changes under realistic conditions, which are inherently far from equilibrium in an operating battery. The majority of *operando* PXRD battery studies are conducted at synchrotron facilities, which offer high brilliance and high X-ray energies. However, access to synchrotron beamtime is for most researchers relatively limited and does not allow for optimization of experiment conditions or screening of a large number of materials, which is often useful within an iterative research or development process. Hence, the use of in-house X-ray diffractometers for *operando* experiments is extremely beneficial as it provides easy and flexible access to *operando* PXRD data.

Several battery cells have been demonstrated for *operando* PXRD experiments. The cells are typically based on a Swagelok™, coffee bag or coin cells in which X-ray transparent window have been implemented by various means. Cells for synchrotron studies typically operate in transmission mode. Examples of *operando* battery cells applied at synchrotrons are found in refs. [10–14].^[5] However, designs and modifications of synchrotron cells for *operando* laboratory PXRD experiments have also been demonstrated. These are mostly based on Bragg-Brentano geometry (reflection mode) due to the low penetration of the commonly employed low energy in-house X-rays (e.g. Cu-K α radiation). For example, in 2014, Shen et al.^[6] published a new cell designed for *operando* experiments in reflection geometry, and in 2020 Wilson et al.^[7] demonstrated how a modified coin cell with a Kapton polyimide window on the positive electrode

[a] M. Johansen, J. K. Verdelin, T. O. Kessler, Prof. D. B. Ravnsbæk
Centre for Integrated Materials Research, Department of Chemistry, Aarhus University, Langelandsgade 140, DK-8000 Aarhus C, Denmark
E-mail: dorthe@chem.au.dk

[b] A.-J. Kallio, Prof. S. Huotari
Department of Physics, University of Helsinki, P. O. Box 64, FI-00014 Helsinki, Finland

[**] DANOISE: Developed in Aarhus: New Operando In-house Scattering Electrochemical

 Supporting information for this article is available on the WWW under <https://doi.org/10.1002/batt.202400033>

 © 2024 The Authors. Batteries & Supercaps published by Wiley-VCH GmbH. This is an open access article under the terms of the Creative Commons Attribution License, which permits use, distribution and reproduction in any medium, provided the original work is properly cited.

side also works for reflection mode. While reflection geometry offers the advantage of only probing the relevant electrode, it holds the drawback of probing the side of the electrode pointing away from the point of reaction, which can result in delayed observation of the phase transition.^[8]

With recent improvements in both detectors and X-ray sources of laboratory diffractometers, in-house *operando* battery studies become increasingly relevant. One of many interesting developments is the emergence of commercial diffractometers for total scattering experiments and pair distribution function analysis. Due to the requirement for high-quality data collected to high scattering angles (or high momentum transfer, Q), these instruments are usually equipped with high-energy X-ray sources, such as an Ag-K_α source ($\lambda = 0.5594 \text{ \AA}$, 22 keV), and high-end detectors covering large angular ranges. This combination provides relatively high X-ray penetration power and fast data collection when only the Bragg reflections need to be considered. Hence, the total scattering diffractometers open new possibilities for *operando* PXRD using transmission battery cells, which resemble those typically utilized at synchrotron facilities. Examples of such instruments are the STOE STADI P and Panalytical Empyrean.

In this work, we set out to construct, test and validate a battery cell for *operando* transmission PXRD studies at an Ag-source in-house diffractometer. The cell should be able to deliver PXRD of a quality suitable for Rietveld refinement to obtain at least changes in unit cell parameters and positions of the first-row transition metals. As it is well-known that cells suitable for PXRD can also be used for X-ray absorption spectroscopy (XAS),^[5a,b] we also aimed to perform preliminary XAS experiments to investigate the performance of the cell for in-house X-ray absorption near edge spectroscopy (XANES). During the recent decade the interest in laboratory XAS has increased as various laboratories^[9] and companies such as EasyXAFS LLC, HP Spectroscopy GmbH and Sigray Inc have optimized their instrument designs. The relationship between laboratory XAS spectrometers and synchrotron XAS beamlines have been discussed in detail by Ditter et al.^[9a] Most notably for battery studies, laboratory XAS enable long term studies where one can cycle the battery material far longer than what is

possible during short synchrotron beamtimes as demonstrated in 2019 by Jahrman et al.^[10a] and in 2022 by Lahtinen et al.^[10b] The same holds for other types of *operando* chemical reactions such as catalysis.^[11] However, most of the battery studies have been conducted using pouch cells,^[10] and while some self-designed cells have been showcased,^[12] the field is still in its infancy.

Herein we demonstrate a new battery cell for transmission *operando* laboratory based PXRD and XAS. The cell is named the "Developed in Aarhus: New Operando In-house Scattering Electrochemical cell – in short, the DANOISE cell. We describe the design of the cell, test and optimize its abilities in terms of diffraction and electrochemical performance, and finally we demonstrate use of the DANOISE cell for *operando* PXRD and XANES through two Li-ion and one Nafion battery case studies.

Experimental

Materials Used for Cell Construction

The DANOISE cell (Figure 1) casing was designed using the FUSION 360 software (AUTODESK Inc.) and 3D printed with a non-resistant polylactic acid (PLA) filament (Banbu lab or Devil Design) using either a Ultimaker S5 or Bambu lab P1P 3D printer. X-ray transparent SIGRADUR® G glassy carbon discs with a diameter of 20 mm and thickness of 300 and 500 μm were delivered by the German company Hochtemperatur-Werkstoffe GmbH. Electrical contact to the glassy carbon discs were ensured either by glueing them into the cell body using conductive Ag-epoxy (JSD-856YQ, Jaston), or by use of pogo pins (KYOCERA AVX, 709150001020006). In the latter case, the discs were glued in using regular fast drying epoxy glue (Epoxy Rapid 332, Dana Lim). The external 2 mm banana jacks were made from brass turned on a lathe while the 2 mm banana plug is a gold-plated banana plug.

Battery Preparation and Electrochemistry

Cathodes pellets were prepared by mixing active material (LiFePO₄, LiNi_{1/3}Mn_{1/3}Co_{1/3}O₂ or P2-Na_{0.67}Fe_{0.5}Mn_{0.5}O₂), conductive carbon, i.e., graphite (C-nergy SFG6L, IMERYS), acetylene black (VXC72, Cabot corporation), and polyvinylidene fluoride binder

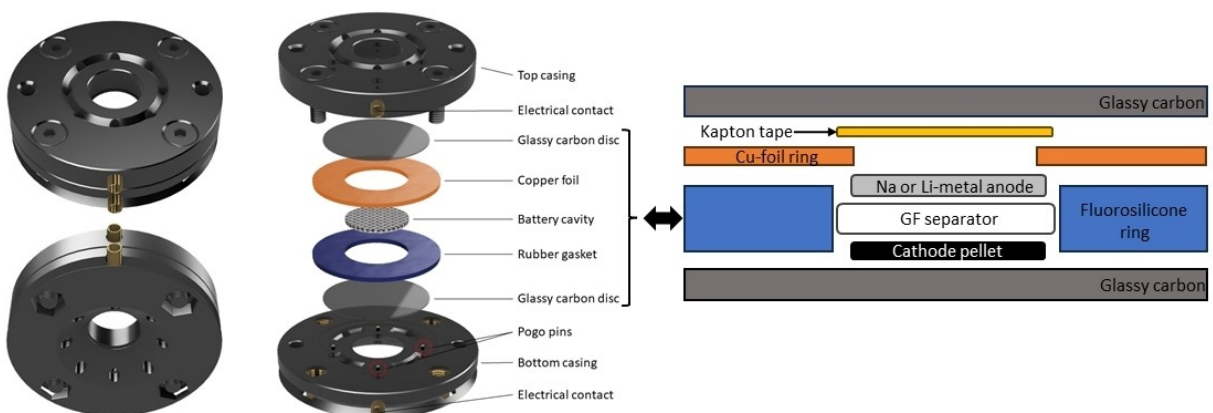


Figure 1. (Left) Illustration of the DANOISE cell shown as closed from both sides (leftmost) and an expanded view with the stack parts (middle). (Right) Illustration of the battery stack cross-section.

(PVdF, HSV900, MIT) in mass ratios of 60:15:15:10, 70:10:10:10, 80:5:5:10 and 90:0:0:10. The mixtures were thoroughly ground using mortar and pestle. The pellet mixture was pressed into free-standing pellets of Ø7 mm pellet weighing 12–15 mg or Ø10 mm weighing either 25–30 or 35–40 mg, using a uniaxial hydraulic press at 1.8 metric tonnes for one minute. The height of two pellets with masses 25.3 and 39.7 mg were determined to 240 and 380 µm, respectively. Using free-standing pellet electrodes instead of electrodes cast onto Al- or Cu-current collectors eliminates the strong Bragg reflections otherwise caused by the metal foils.

The free-standing electrode pellets were mounted in battery stacks in the DANOISE cell or in standard coin cells. The Li-ion electrodes, LiFePO₄ (LFP) and LiNi_{1/3}Mn_{1/3}Co_{1/3}O₂ (NMC111), were mounted against a Li-metal anode using a 1 M solution of lithium hexafluorophosphate (LiPF₆, Solvionic, 99.9%, ethylene carbonate:dimethyl carbonate 1:1, v/v) electrolyte. The Na-ion electrode, P2-Na_{0.67}Fe_{0.5}Mn_{0.5}O₂, was mounted against a Na-metal anode with a 1 M solution of sodium bis(trifluoromethanesulfonyl)imide (NaTFSI, Solvionic, 99.9%, ethylene carbonate:dimethyl carbonate 1:1, v/v) as electrolyte. In all cases, Whatman GF/B separators (680 µm thick) were used. All cells were assembled in an argon-filled glovebox equipped with circulation purification.

The batteries were cycled at current rates between C/10 and C/20 within potential limits of 2.5–4.2 V for LiFePO₄, 3.0–4.4 V for LiNi_{1/3}Mn_{1/3}Co_{1/3}O₂ and 1.5–4.3 V for P2-Na_{0.67}Fe_{0.5}Mn_{0.5}O₂.

Powder X-Ray Diffraction

All diffraction data was collected with the battery stack mounted in the DANOISE cell on a STOE STADI P diffractometer using Ag K_{α1} ($\lambda=0.5594\text{ \AA}$) radiation and MYTHEN 1K detectors. The size of the slitted beam was 6x1.3 mm². *Operando* PXRD measurements were conducted using five minutes exposure per pattern. The batteries were cycled at a C/20 current rate.

Rietveld refinement was conducted using the FullProf suite using a Thompson-Cox-Hastings with axial divergence peak profile.^[13] All data has been analysed in 2θ but are presented in Q (Q = $\frac{4\pi}{\lambda} \cdot \sin(\theta)$) to ease comparison with literature and measurements using other wavelengths and instruments. Crystal structures have been visualized and modified using VESTA.^[14]

The agreement factor, R_{wp}, are calculated using Eq. 1 where, w, is the weight of the observed intensity, y, and calculated intensity, y_c. The values are not corrected for background.

$$R_{wp} = 100 \left[\frac{\sum_{i=1,n} w_i |y_i - y_{c,i}|^2}{\sum_{i=1,n} w_i y_i^2} \right]^{1/2} \quad (1)$$

X-Ray Absorption Spectroscopy

X-ray absorption measurements were conducted using HelXAS spectrometer at the Center for X-ray Spectroscopy at the University of Helsinki.^[9b] The Rowland circle spectrometer consists of a Johann-type spherically bent crystal analyser (SBCA), 1.5 kW Ag anode water-cooled X-ray source with 0.4x0.8 mm² source size, and Amptek X-123 silicon drift diode detector with 70 mm² active area. The monochromator used to collect Fe spectra was Si(531) which at Fe K-edge 7.112 keV has a Bragg angle of 71.74°. As a scan, we used 7.09–7.18 keV and divided this range into 240 scan points, resulting in 0.375 eV steps, and each scan point was measured for

0.5 seconds, including deadtime and readout time resulted in a total scan time of ~16 minutes per spectrum. The measured spectra were background subtracted and area normalized. The DANOISE cell was mounted in front of the detector in a 3D printed holder held in place by four magnets to enable fast exchange of the cell. The I₀ was measured by removing the cell in front of the detector. The cell was connected to a home-built galvanostat comprised of an Arduino-based relay board, a MASTECH MS7221 calibrator to deliver power and a multimeter.

The Bragg angle of the Fe K-edge using a Si(531) analyser is quite an extreme case with a low angle resulting in very long beam in the nondispersive direction, which is much larger than the diameter of the active area. As the shape of the beam is the same for I₀ scans, the elongation does not affect the shape of the measured spectrum but some of the flux is lost. In this case one could have considered to use Ge(620) analyser but with accelerating voltage above 10 kV the fluorescence lines of Ge will be illuminated, and this will saturate the detector. The high-power X-ray generator used for this work is specified to use 2 mA current at 10 kV accelerating voltage resulting in total power of 20 W but with 20 kV it is possible to use 40 mA current resulting in 800 W accelerating power.

Results and Discussion

Design of the DANOISE Cell

Battery cells for *operando* X-ray scattering and absorption experiments need to satisfy a set of requirements:

1. All cell components must be made from materials, which are chemically inert towards the electrodes and electrolyte within the operating potential range used in the experiments.
2. The cell must protect the battery stack from air or moisture in the surrounding atmosphere,^[6,8] and retain the liquid electrolyte in the cell stack.
3. The cell must be equipped with current collectors providing good electrical contact between the electrodes and the external circuit.
4. The cell must ensure that the two electrodes are electrically insulated from each other.
5. The cell must provide sufficient pressure across the battery stack.
6. The cell must allow sufficient X-ray penetration to collect the scattered and transmitted x-rays with a quality allowing the desired analysis and with a proper time resolution for the charging/discharging time of the battery (i.e., the selected current rate).

The design of the DANOISE cell is shown in Figure 1. The body of the cell, i.e. the top and bottom casings are 3D printed in PLA and equipped with electrical contacts for the external circuit, pogo pins and 300 or 500 µm thick glassy carbon discs in the centre of the casings. Glassy carbon is impenetrable to air and moisture, electrically conductive (specific electrical resistance of $45 \cdot 10^{-4}\text{ }\Omega\text{-cm}$), rigid and a low Z material. Thus, it fulfils requirements 2, 3, 5 and 6. Hence, the properties of glassy carbon allow it to serve both as an X-ray window and a current collector. A drawback of glassy carbon is that while it is hard, it is, like most glasses, also

brittle. Therefore, the DANOISE cell employs Ø20 mm carbon discs, which allows for a large support area in the casing for the discs to rest on. This prevents them from cracking when the cell is closed and tightened. On the outside of the DANOISE cell, the window has a diameter of Ø10 mm ensuring that the larger X-ray beams (compared to synchrotron X-ray beams) can be utilized. To optimize the angular range of the collected PXRD data at the energy of Ag K_{a1} ($\lambda = 0.55941 \text{ \AA}$), the cell was designed with an opening angle of $\sim 50^\circ$ 2θ ($\sim 9.5 \text{ \AA}^{-1}$), allowing for high Q measurements if tilting/rotating the cell with the goniometer stage.

To obtain good electrical contact between the glassy carbon and the electrical contact in the casing, either Ag-epoxy or pogo pins were employed. Pogo pins are spring-loaded pins that ensure contact when the top and bottom casings of the cell are pushed together. Glassy carbon is known to be inert towards the cathode and electrolyte (requirement 1). However, Li-ion intercalation can occur on the anode side. Hence, the anode-side window is covered with a thin disc of protective Kapton tape.^[5a] As Kapton is not conductive, a donut-shaped piece of copper foil is placed between the anode and the Kapton to ensure electrical contact between the anode and the glassy carbon. Note, that for this to work the diameters (\varnothing) must be so that $\varnothing_{\text{outer, copper}} \geq \varnothing_{\text{glassy carbon}} > \varnothing_{\text{Kapton}} > \varnothing_{\text{inner, copper}}$ and $\varnothing_{\text{anode}} > \varnothing_{\text{inner, copper}}$ (see Figure 1, right). Finally, a rubber gasket made from fluorosilicone (fluoro vinyl methyl silicone,

FVMQ) encloses the battery stack in the centre of the cell. This both prevents air and moisture from reaching the stack and ensures that the cell do not short circuit by the top and bottom current collectors touching each other.

Optimization of X-Ray Diffraction Data Quality

Before constructing the cell, a series of proof-of-concept X-ray diffraction measurements were done in a mock-up cell with 500 μm thick glassy carbon windows (Figure S1). The tests were designed to inspect the quality of the PXRD data obtained from the cell containing a complete battery stack with an electrode at different states-of-charge (SOC). Thus, a set of LFP cathodes (w. mass ratio of LFP:conductive carbon:binder = 60:30:10) were charged to 25%, 50%, 75% and 100% state-of-charge in a Swagelok half-cell and transferred to the mock-up cell. After only five minutes of X-ray exposure, PXRD data of a quality suitable for Rietveld refinement (Figure 2) were obtained. Note that the weight fractions of LFP and FP correspond well to those expected from the state-of-charge. A time resolution of five minutes is adequate for battery cycling at current rates of $\leq C/10$, i.e., a current rate of C/10 provides full charge or discharge in 10 hours, i.e., 120 PXRD patterns will be obtained during both charge and discharge, and more importantly the

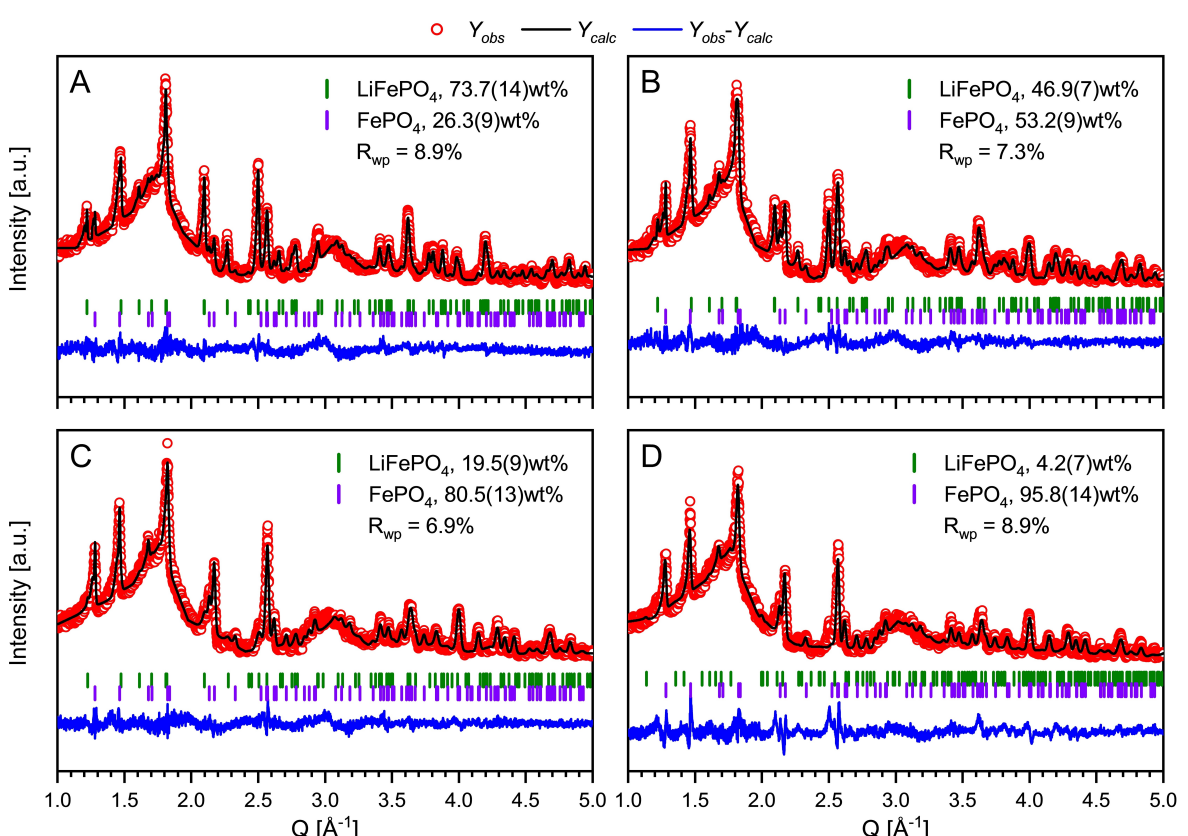


Figure 2. Rietveld refinement of PXRD data from $\text{Li}_x\text{FePO}_4/\text{Li}$ battery stacks in the DANOISE cell. The cells were charged to selected SOC prior to the PXRD measurements, i.e. SOCs of A) 25%, B) 50%, C) 75% and D) 100% SOC. The number of refined parameters was kept low to simulate a situation comparable to sequential refinement. Note that 500 μm thick glassy carbon windows were used for these initial experiments.

state-of-charge will change only 0.83% during collection of one pattern.

The PXRD data obtained in this first test contains strong diffuse signals (e.g., at $Q \sim 1.7$ and 3.1 \AA^{-1}) from the glassy carbon, which is henceforth referred to as the background. The background particularly at $\sim 1.7 \text{ \AA}^{-1}$ arises from the carbon window and additives, i.e. structural motifs from graphite with equidistant layers stacked parallel to each other with a high degree of orientational disorder.^[15] To minimize this, the 500 μm carbon windows were exchanged for thinner ones of 300 μm . This, as expected, clearly reduced the background level (Figure 3).

To further enhance the signal-to-noise (S/N) ratio of the PXRD data, the amount of active material in the beam, i.e., the electrode composition and thickness, was optimized bearing in mind that the electrode must still deliver satisfying electrochemical performance. First, the effects of altering the composition of the electrode, i.e., the pellet mix, were investigated by testing electrodes with varying LFP:conductive carbon mass ratio. A constant PVdF-binder content of 10 wt.% was used as this is required for making mechanically robust free-standing pellets (note that the amount of binder may be decreased for other active materials). Naturally, increasing the content of the active material increases the Bragg intensities, and the optimal fit is obtained for the 80:10:10 sample (Figure 4). However, decreasing the amount of conductive carbon inherently decreases the electrical conductivity in the electrode composite, as the active inorganic electrode materials typically have poor electrical conductivity. As expected, poor electrochemical performance is observed when the amount of active material in the electrode exceeds 70 wt.% (Figure S2). Fortunately, for the 70:20:10 electrode, the scattering data is still of good quality with a S/N of 7.7 compared to 7.0 and 8.8 for the 60:30:10 and 80:10:10 compositions, respectively. Hence, the 70:20:10 composition is a good standard for *operando* experiments using

the DANOISE cell on an Ag-source instrument. Secondly, the effects of varying the thickness of the electrode pellets were inspected. The thicknesses were varied by changing the mass of the electrode pellets from 25–30 to 35–40 mg, while keeping the diameter fixed at 10 mm. As expected, the thicker electrodes provide a higher quality PXRD data (Figure 5), i.e., the background level is constant as this mainly arise from the carbon windows, but the signal-to-noise ratio is increased from 6.6 to 7.7 for pellet of the 70:20:10 composition. As the electrochemical performance was not found to suffer from increasing the thickness of the electrodes (Figure S3) at the current rates relevant for the *operando* experiments (i.e., C/10 or lower), an electrode mass of 35–40 mg is advised for use of the DANOISE cell.

Finally, to compare PXRD from different electrode materials a series of the commonly employed types of materials were tested, i.e., $\text{LiNi}_{1/3}\text{Mn}_{1/3}\text{Co}_{1/3}\text{O}_2$ (NMC), $\text{Li}_4\text{Ti}_5\text{O}_{12}$ (LTO) and P2- $\text{Na}_{0.67}\text{Fe}_{0.5}\text{Mn}_{0.5}\text{O}_2$ (NaFM) and compared to LFP (Figure 6). For all materials, the data quality is sufficient to extract information about the unit cell parameters and atomic positions (except for Li) by Rietveld refinement.

We note that the major challenge encountered during Rietveld refinement of the data was modelling the effects from the axial divergence arising from the geometry of the diffractometer (mainly the 50 μm wide silicon strips), e.g., in Figure 6 all refinements show undescribed intensities in the difference curve, ascribed to the remaining artefacts from the axial divergence contribution.

Validation of the Electrochemical Performance

Optimizing the diffracted X-ray signal from the *operando* battery cell, naturally has no real value if the electrochemical performance is not reliable or representative of the conditions

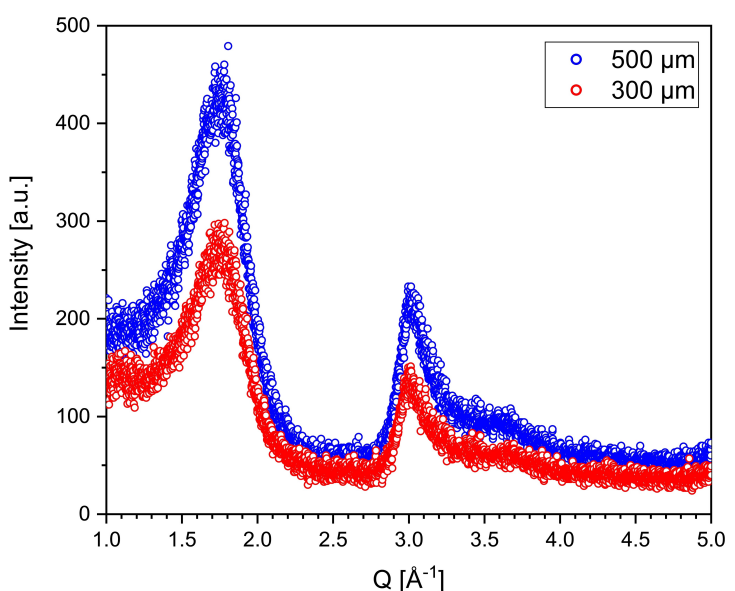


Figure 3. Comparison of the background contribution from 300 (red) and 500 μm (blue) glassy carbon windows.

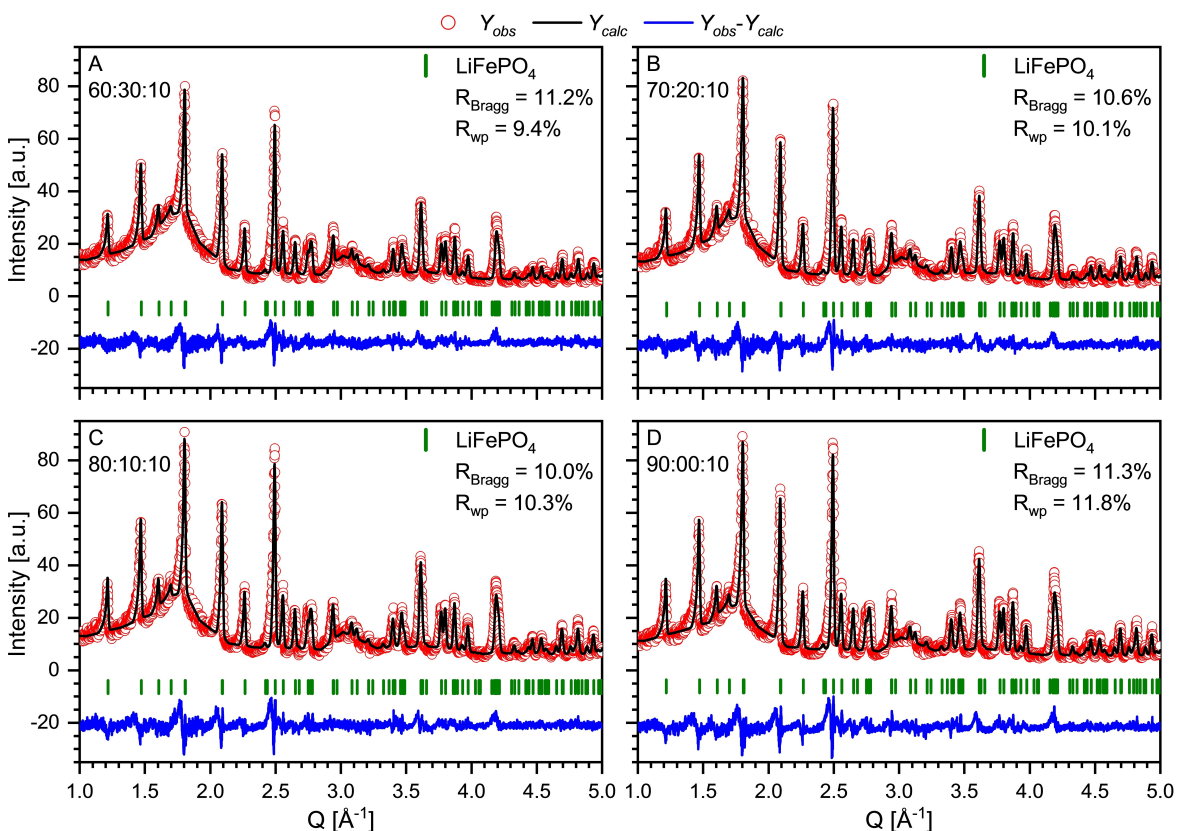


Figure 4. Rietveld refinement of PXRD data from LiFePO₄/Li battery stacks in the DANOISE cell with electrode pellets with varying mass ratio of LiFePO₄:Conductive carbon:PVdF of A) 60:30:10, B) 70:20:10, C) 80:10:10 and D) 90:00:10.

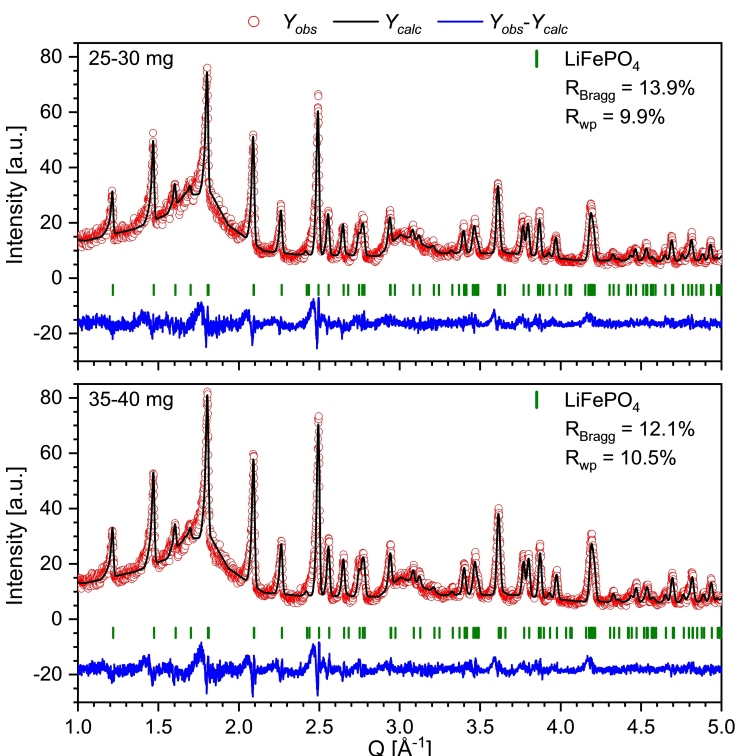


Figure 5. Rietveld refinement of PXRD data from LiFePO₄/Li battery stacks in the DANOISE cell with electrode pellets with varying masses of 25–30 mg (top) and 35–40 mg (bottom).

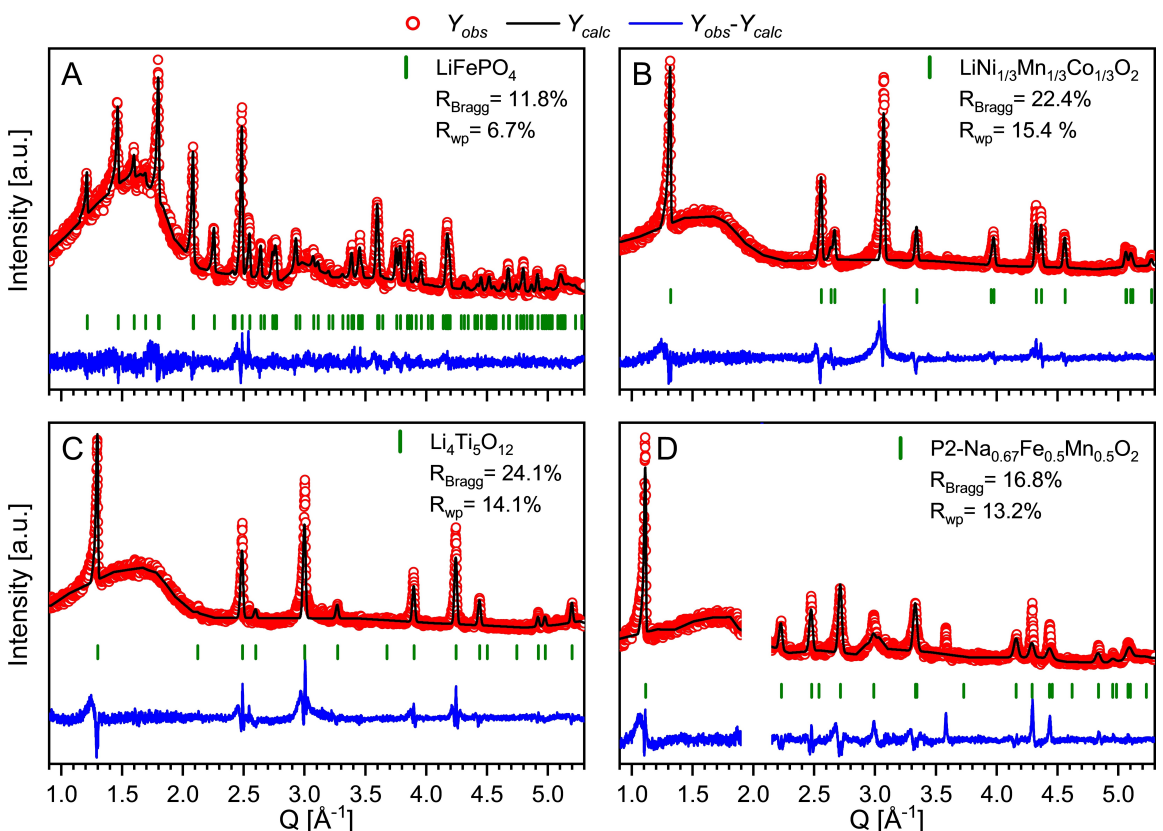


Figure 6. Rietveld refinement of PXRD data from the DANOISE cell with battery stacks containing different active materials, i.e., A) LiFePO₄, B) Li₄Ti₅O₁₂, C) LiNi_{1/3}Mn_{1/3}Co_{1/3}O₂ and D) P2-Na_{0.67}Fe_{0.5}Mn_{0.5}O₂. In the diffraction signal for the P2-Na_{0.67}Fe_{0.5}Mn_{0.5}O₂ cell, peaks are observed around 2 Å⁻¹ from the Na-metal anode. This has been omitted by excluding the relevant angular range.

in common battery format, e.g., a coin cell. To validate the electrochemical performance of the DANOISE cell during galvanostatic charge-discharge cycling, which is the typical mode in *operando* experiments, a set of identical LFP half-cells was mounted in a coin cell and in two DANOISE cells: one with pogo-pins and one with Ag-epoxy. The cells were subjected to galvanostatic intermittent titration technique (GITT) experiments (Figure 7), which shows that the overpotential is comparable for the coin cell and DANOISE cells as well as for the two types of connectors (pogo-pins and Ag-epoxy) used in the DANOISE cells. The coin cell delivers a slightly higher capacity than the DANOISE cell, likely due to a higher stack pressure in the coin cell.

Finally, to evaluate the ability of the DANOISE cell to perform multiple charge-discharge cycles, a standard galvanostatic experiment was conducted using a current rate of C/20 (Figure 7). The DANOISE cell delivers stable capacities for the first five cycles, which equivalates to ~176 hours of operation. After this point, the capacity rapidly decreases and after 12 cycles the cell is not capable of delivering any capacity at all. The capacity fade is mainly subscribed to the cell not being completely leak-free, i.e., the cell continuously loose electrolyte.

Examples of *operando* PXRD Data

To validate the combined electrochemical and PXRD performance of the DANOISE cell, two commercial electrode materials with well-established electrochemical and structural charge-discharge behaviour were selected for *operando* PXRD experiments, i.e., LiFePO₄ (LFP) and LiNi_{1/3}Mn_{1/3}Ni_{1/3}O₂ (NMC111). These materials also represent two types of cathode materials, with LiFePO₄ belonging to the olivine family (one-dimensional Li-migration) and NMC(111) belonging to the family of layered material (two-dimensional Li-ion migration). Furthermore, as proof of concept, we investigate the capabilities of the DANOISE cell for studies of Na-ion batteries through the investigation of a layered P2-Na_{0.67}Fe_{0.5}Mn_{0.5}O₂ material. The crystal structures of the three materials used for the *operando* measurements below are depicted in Figure 8.

Olivine LiFePO₄ for Li-ion Batteries

Olivine LiFePO₄ has a well-established biphasic behaviour when extracting and intercalating Li-ions in the structure. The biphasic transition results in LiFePO₄ gradually transforming to FePO₄. At low current rates (like that employed here), there is only a very narrow solid solution regime near the endmembers, and the unit cell parameters are thus almost constant for the

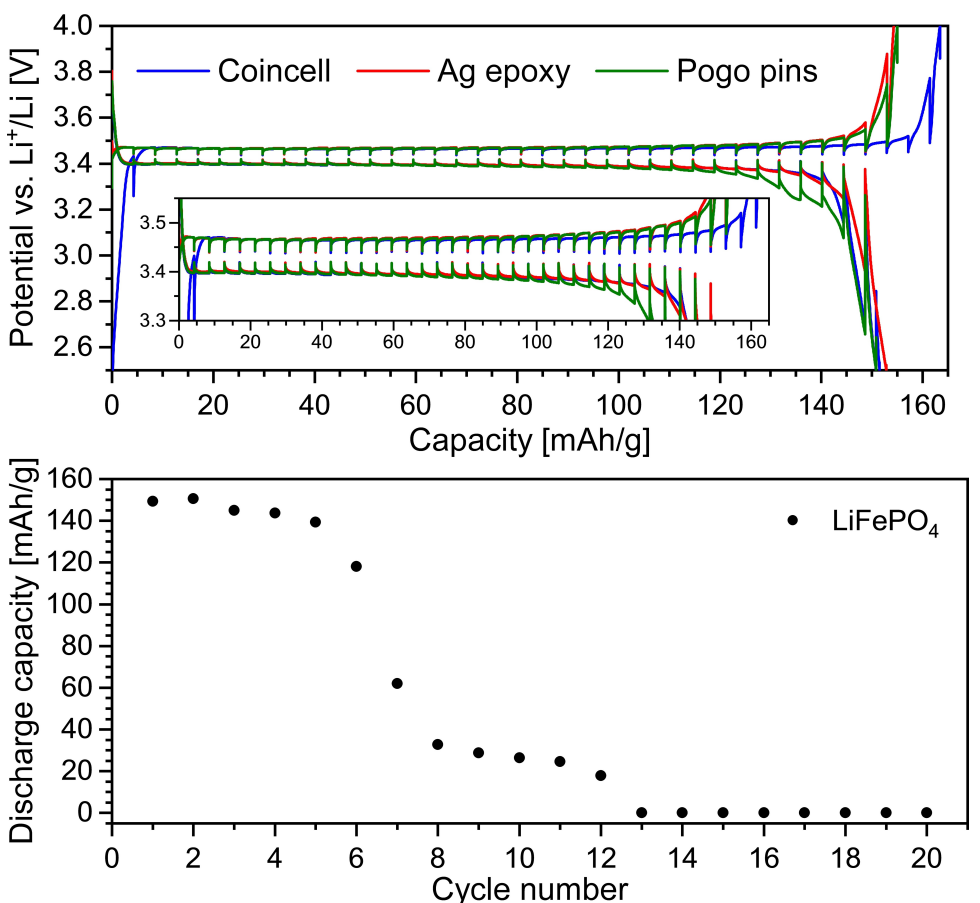


Figure 7. (Top) GITT and (Bottom) galvanostatic stability tests performed on LiFePO₄-Li battery stacks at C/20 current rates. GITT measurements compare the performance of a coin cell to the DANOISE cell with contact through Ag-epoxy or pogo pins. The stability test is performed only on the DANOISE cell with pogo pins.

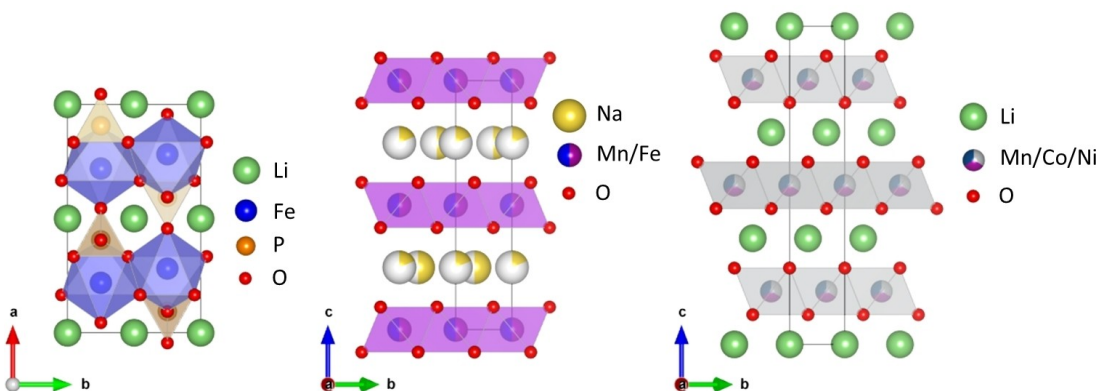


Figure 8. Crystal structures of LiFePO₄ (left), LiNi_{1/3}Mn_{1/3}Co_{1/3}O₂ (centre), and P2-Na_{0.67}Fe_{0.5}Mn_{0.5}O₂ (right). Crystal structures are obtained from The Materials Project.^[16]

two phases throughout the charge-discharge process. This also means that the weight fraction of FePO₄ is proportional to the SOC.

The *operando* PXRD (Figure 9) confirms the biphasic LiFePO₄ \leftrightarrow FePO₄ phase transition, which follows the electrochemical progress as expected. However, some asymmetry is observed in the behaviour of the phase fractions, i.e., the structural

conversion is somewhat delayed compared to the electrochemical state-of-charge. Similar behaviour has been observed in other *operando* studies^[17] and may be caused by solid-solution behaviour, intermediate amorphization or weak beam damage.^[18] The asymmetry is more evident during charge than during discharge.^[1c,19] The electrochemistry shows that >1 Li-ion is intercalated during discharge. As this is not possible in

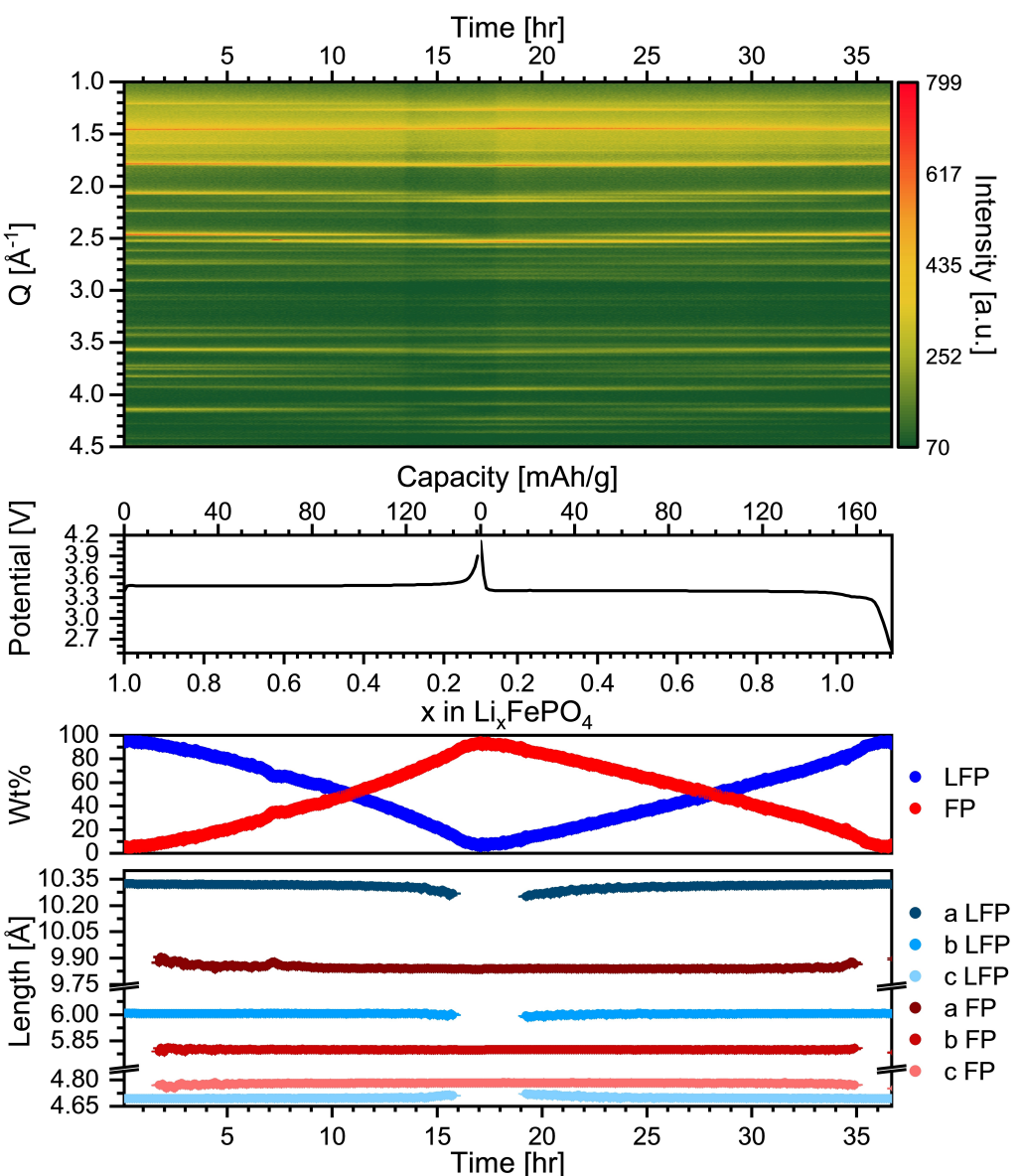


Figure 9. (Top) Background subtracted contour plot of *operando* PXRD of LiFePO_4 , and (middle) the simultaneously collected potential profile for the galvanostatic charge and discharge as a function of capacity and overall Li-content in the electrode, i.e., x in Li_xFePO_4 . (Bottom) Weight fractions and unit cell parameters for LiFePO_4 and FePO_4 extracted by Rietveld refinement. Note, the unit cell parameters were not refined for phase content below 10 wt.%.

LFP, an unexpected side reaction, contributing to the current drawn from the battery, occur during discharge. This is likely the reason for the additional plateau observed at ~ 3.3 V and $x > 1$ during discharge. This may be caused by unexpected exposure to air or moisture.

Layered $\text{LiNi}_{1/3}\text{Mn}_{1/3}\text{Co}_{1/3}\text{O}_2$ for Li-ion Batteries

The *operando* PXRD of the layered NMC111 (Figure 10) shows a single-phase solid solution behaviour throughout the charge-discharge process, which is well in line with previous reports.^[20] As lithium ions are slowly extracted from the structure during charge, the unit cell slowly expands along the stacking direction corresponding to an increase in the c -direction. This expansion

is explained by electrostatic repulsion between the transition metal (TM) oxide layers being decreasingly shielded by Li-ions. However, near the end of the charge, the c -direction starts to decrease due to the reduced TM–O bond lengths caused by the oxidation of the transition metal. The structural behaviour is highly comparable to results presented by O. Dolotko^[20a] based on their finding from an *operando* neutron diffraction experiment.

Layered P2- $\text{Na}_{0.65}\text{Fe}_{0.5}\text{Mn}_{0.5}\text{O}_2$ for Na-Ion Batteries

Na-ion batteries are a promising, sustainable, and cheap alternative to Li-ion batteries, and there is a lot of incentive to investigate phase transitions under *operando* conditions in Na-

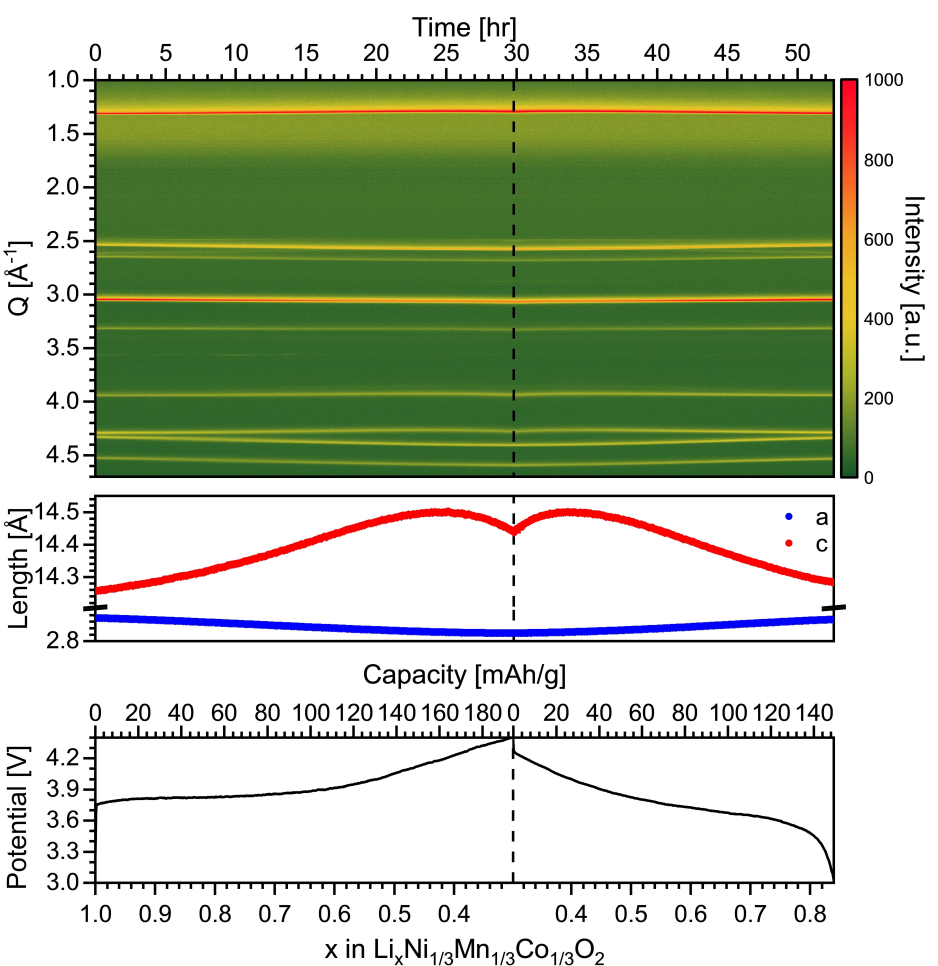


Figure 10. (Top) Background subtracted contour plot of *operando* PXRD of $\text{LiNi}_{1/3}\text{Mn}_{1/3}\text{Co}_{1/3}\text{O}_2$ correlated to the (middle) state of charge as x in $\text{Li}_x\text{Ni}_{1/3}\text{Mn}_{1/3}\text{Co}_{1/3}\text{O}_2$ and (bottom) capacity calculated from time and current.

ion battery materials.^[21] Hence, it is highly relevant to test if the DANOISE cell allows for *operando* studies of Na-ion batteries, which are more demanding as the Li-anode is replaced by a Na-anode, which interacts more with the X-rays. For the test, we utilize a P2- $\text{Na}_{0.65}\text{Fe}_{0.5}\text{Mn}_{0.5}\text{O}_2$ cathode material. The letter “P” refers to the Na-ions sitting in a prismatic oxygen environment and the number “2” refers to the number of transition metal oxide layers in the unit cell, i.e., the stacking sequence. The nomenclature was introduced by Delmas, et al.^[22] This P2-material has recently been studied by Drejer, et al.^[23] using synchrotron based *operando* PXRD utilizing an AMPIX cell.^[5a]

The *operando* PXRD data obtained from the DANOISE cell (Figure 11) show an almost identical behaviour to that reported by Drejer, et al.^[23] At $x \sim 0.35$, P2- $\text{Na}_x\text{Fe}_{0.5}\text{Mn}_{0.5}\text{O}_2$ transforms to OP4- $\text{Na}_x\text{Fe}_{0.5}\text{Mn}_{0.5}\text{O}_2$ (O denotes octahedral Na-coordination), which behaves like a solid-solution for the remainder of the charge process. Note, that the Bragg intensities continuously decrease for OP4-phase due to increasing disorder caused by stacking faults. Upon discharging, the P2-phase is recovered at $x \sim 0.45$. Continued discharge leads to intercalation of more Na-ions than the amount present in the synthesized material, i.e., x goes beyond 0.67. At $x \sim 0.8$, the P2-structure undergoes a rearrangement into an orthorhombic distorted phase, denoted

P’2, observed particularly by the emergence of a Bragg peak at $Q \sim 2.5 \text{ \AA}^{-1}$. This phase transition is caused by Jahn-Teller distortions.^[23]

X-ray Absorption Spectroscopy on Olivine LiFePO_4

Being able to use the same *operando* cell for multiple characterization techniques is a huge advantage as it ensures data collection under identical electrochemical conditions. XANES is a strong tool for investigating the valence changes and changes in the coordination geometry while the electrode is active. Thus, to enhance the versatility of the DANOISE cell, a proof-of-concept *operando* XANES measurement has been conducted and is presented here. The LFP/FP system is ideal for the proof-of-concept experiment due to the big shift in the edge energy when the $\text{LiFe}^{2+}\text{PO}_4$ phase transforms into the $\text{Fe}^{3+}\text{PO}_4$ phase.^[24] The edge position changes about 4 eV from 7.119 to 7.123 keV corresponding well with previous reports.^[24b] For the *operando* experiments, the applied acquisition time provides decent XANES data and makes it possible to perform *operando* experiments with an acceptable time resolution at current rates lower than C/10. The data (Figure 12) shows a linear shift in the

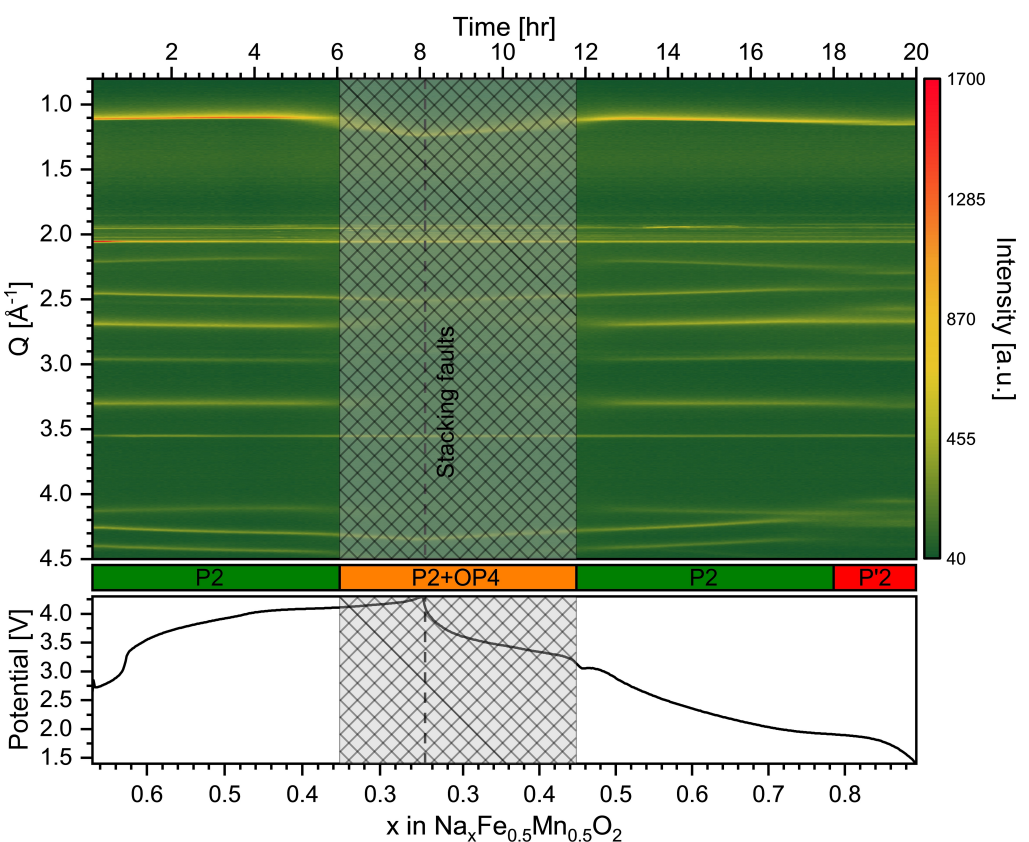


Figure 11. (Top) Background subtracted contour plot of *operando* PXRD of P2- $\text{Na}_{0.67}\text{Fe}_{0.5}\text{Mn}_{0.5}\text{O}_2$ correlated to the (bottom) state of charge as x in P2- $\text{Na}_x\text{Fe}_{0.5}\text{Mn}_{0.5}\text{O}_2$ and capacity calculated from time and current at a C/20 cycling rate.^[23]

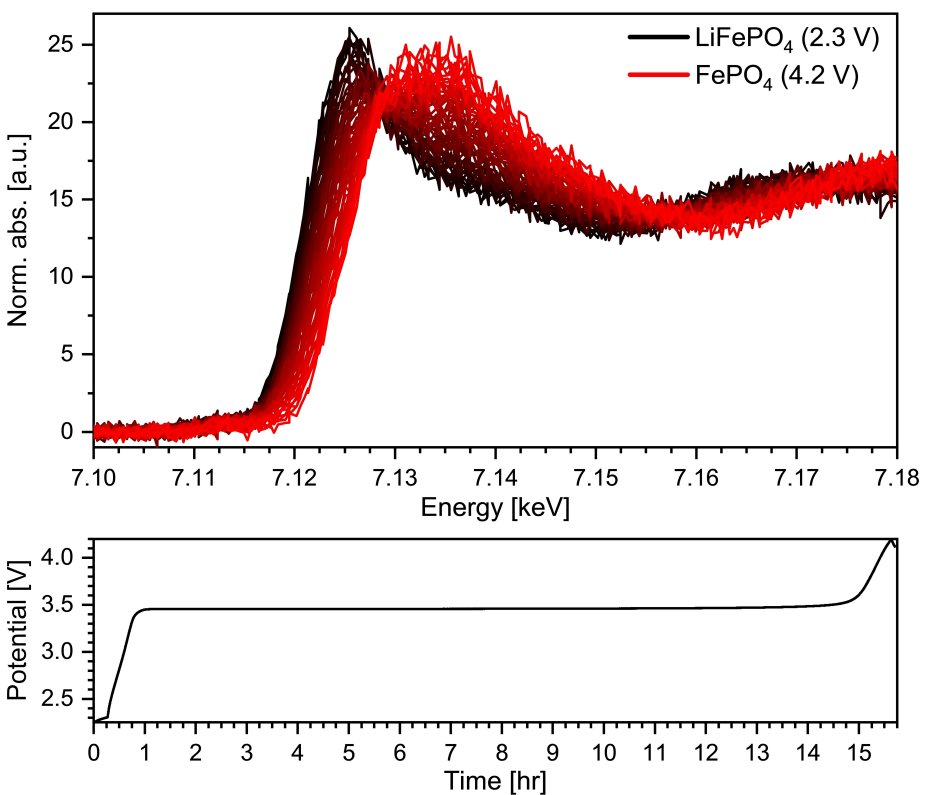


Figure 12. (Top) Normalized XANES spectra and (bottom) the galvanostatic potential profile collected during charge of LiFePO₄ vs. Li at C/15.

edge energy and provides a nice insight into the shift of the K-edge energy and the changes in the local geometry, i.e., based on the absent pre-edge feature, Fe is, as expected, octahedrally coordinated in both the charged and discharged phase and the first oscillation after the white line indicates no clear changes in the ligands of Fe.

Conclusions

Laboratory X-ray instrumentation is improving, making laboratory based *in situ* and *operando* experiments possible. In this work, we described the design, construction and capabilities of the DANOISE cell, which is a new cell for in-house *operando* X-ray diffraction and absorption spectroscopy studies of battery materials. Electrochemical cycling and GITT experiments proved the DANOISE cell to give electrochemical performance comparable to standard coin cells. *Operando* tests on commercial NMC111 and LFP showed solid-solution and biphasic behaviour, respectively, during battery operation, and sequential Rietveld refinement revealed changes in unit cell parameters in good agreement with observations from synchrotron experiments. Using XAS, the expected linear transition from Fe^{2+} to Fe^{3+} upon lithium from LiFePO_4 during battery charge was confirmed using the DANOISE cell. Furthermore, the DANOISE cell was also shown suitable for studies of Na-ion battery materials, i.e. a P2-type layered electrode material showed the expected phase transitions ending in clear broadening of the Bragg reflections due to introduction of stacking disorder, as reported in literature.

Acknowledgements

The authors gratefully thank the Novo Nordic Foundation (Grant No. NNF20OC0062068) for funding this research. Our gratitude goes to Dr. Andreas Østergaard Drejer for providing the material and help on the work related to the layered $\text{P}2\text{-Na}_{0.67}\text{Fe}_{0.5}\text{Mn}_{0.5}\text{O}_2$ phase. Special thanks to dir. René Bess for his valuable supervision and contributions on design and sample preparation for lab-XAS experiments. We acknowledge the Helsinki Center for X-ray Spectroscopy for providing experiment time and support with the HelXAS spectrometer under Proposal number 2022-0014 and 2023-0003.

Conflict of Interests

The authors declare no conflict of interest.

Data Availability Statement

The data that support the findings of this study are available from the corresponding author upon reasonable request.

Keywords: X-ray absorption spectroscopy • X-ray diffraction • Electrochemistry • Intercalations

- [1] a) M. Fichtner, K. Edström, E. Ayerbe, M. Berecibar, A. Bhowmik, I.E. Castelli, S. Clark, R. Dominko, M. Erakca, A. A. Franco, A. Grimaud, B. Horstmann, A. Latz, H. Lorrmann, M. Meeus, R. Narayan, F. Pammer, J. Ruhland, H. Stein, T. Vegge, M. Weil, *Adv. Energy Mater.* **2021**, *12*; b) P. Gupta, S. Pushpakant, M. A. Haider, S. Basu, *ACS Omega* **2022**, *7*, 5605–5614; c) D. Larcher, J. M. Tarascon, *Nat. Chem.* **2015**, *7*, 19–29.
- [2] C. Liu, Z. G. Neale, G. Cao, *Mater. Today* **2016**, *19*, 109–123.
- [3] a) N. Sharma, W. K. Pang, Z. Guo, V. K. Peterson, *ChemSusChem* **2015**, *8*, 2826–2853; b) D. Liu, Z. Shadike, R. Lin, K. Qian, H. Li, K. Li, S. Wang, Q. Yu, M. Liu, S. Ganapathy, X. Qin, Q. H. Yang, M. Wagemaker, F. Kang, X. Q. Yang, B. Li, *Adv. Mater.* **2019**, *31*, e1806620; c) X. Wei, X. Wang, Q. An, C. Han, L. Mai, *Small Methods* **2017**, *1*.
- [4] a) H. Li, S. Guo, H. Zhou, *J. Energy Chem.* **2021**, *59*, 191–211; b) *Nat. Commun.* **2022**, *13*, 4723.
- [5] a) O. J. Borkiewicz, B. Shyam, K. M. Wiaderek, C. Kurtz, P. J. Chupas, K. W. Chapman, *J. Appl. Crystallogr.* **2012**, *45*, 1261–1269; b) W. R. Brant, D. Li, Q. Gu, S. Schmid, *J. Power Sources* **2016**, *302*, 126–134; c) F. Rosciano, M. Holzapfel, H. Kaiser, W. Scheifele, P. Ruch, M. Hahn, R. Kotz, P. Novak, *J. Synchrotron Radiat.* **2007**, *14*, 487–491; d) J. B. Leriche, S. Hamelet, J. Shu, M. Morcrette, C. Masquelier, G. Ouvrard, M. Zerrouki, P. Soudan, S. Belin, E. Elkaiim, F. Baudelet, *J. Electrochem. Soc.* **2010**, *157*, A606; e) H. Liu, P. K. Allan, O. J. Borkiewicz, C. Kurtz, C. P. Grey, K. W. Chapman, P. J. Chupas, *J. Appl. Crystallogr.* **2016**, *49*, 1665–1673.
- [6] Y. Shen, E. E. Pedersen, M. Christensen, B. B. Iversen, *Rev. Sci. Instrum.* **2014**, *85*, 104103.
- [7] G. Wilson, S. Zilinskaite, S. Unka, R. Boston, N. Reeves-McLaren, *Energy Rep.* **2020**, *6*, 174–179.
- [8] A. V. Llewellyn, A. Matruglio, D. J. L. Brett, R. Jervis, P. R. Shearing, *Condens. Matter* **2020**, *5*.
- [9] a) A. S. Ditter, E. P. Jahrman, L. R. Bradshaw, X. Xia, P. J. Pauzauskie, G. T. Seidler, *J. Synchrotron Radiat.* **2019**, *26*, 2086–2093; b) A. P. Honkanen, S. Ollikkala, T. Ahopelto, A. J. Kallio, M. Blomberg, S. Huotari, *Rev. Sci. Instrum.* **2019**, *90*, 033107.
- [10] a) E. P. Jahrman, L. A. Pellerin, A. S. Ditter, L. R. Bradshaw, T. T. Fister, B. J. Polzin, S. E. Trask, A. R. Dunlop, G. T. Seidler, *J. Electrochem. Soc.* **2019**, *166*, A2549–A2555; b) K. Lahtinen, M. Labmayr, V. Mäkelä, H. Jiang, J. Lahtinen, L. Yao, E. O. Fedorovskaya, S. Rässänen, S. Huotari, T. Kallio, *Mater. Today* **2022**, *27*.
- [11] a) J. G. Moya-Cancino, A. P. Honkanen, A. M. J. van der Eerden, H. Schaink, L. Folkertsma, M. Ghiasi, A. Longo, F. M. F. de Groot, F. Meirer, S. Huotari, B. M. Weckhuysen, *ChemCatChem* **2019**, *11*, 1039–1044; b) J. G. Moya-Cancino, A. P. Honkanen, A. M. J. van der Eerden, H. Schaink, L. Folkertsma, M. Ghiasi, A. Longo, F. Meirer, F. M. F. de Groot, S. Huotari, B. M. Weckhuysen, *ChemCatChem* **2019**, *11*, 3042–3045; c) N. S. Genz, A. J. Kallio, R. Oord, F. Krumeich, A. Pokle, O. Prytz, U. Olsbye, F. Meirer, S. Huotari, B. M. Weckhuysen, *Angew. Chem. Int. Ed.* **2022**, *61*, e20220934.
- [12] V. V. Shapovalov, A. A. Guda, N. V. Kosova, S. P. Kubrin, O. A. Podgornova, A. M. Aboraia, C. Lamberti, A. V. Soldatov, *Radiat. Phys. Chem.* **2020**, *175*.
- [13] a) J. Rodríguez-Carvajal, *Physica B: Condensed Matter* **1993**, *192*, 55–69; b) J. Rodríguez-Carvajal, *IUCr Newsletter* **2001**, *26*, 12–19.
- [14] K. Momma, F. Izumi, *J. Appl. Crystallogr.* **2011**, *44*, 1272–1276.
- [15] J. Biscoe, B. E. Warren, *J. Appl. Phys.* **1942**, *13*, 364–371.
- [16] A. Jain, S. P. Ong, G. Hautier, W. Chen, W. D. Richards, S. Dacek, S. Cholia, D. Gunter, D. Skinner, G. Ceder, K. A. Persson, *APL Mater.* **2013**, *1*, 011002.
- [17] Y.-H. Kao, M. Tang, N. Meethong, J. Bai, W. C. Carter, Y.-M. Chiang, *Chem. Mater.* **2010**, *22*, 5845–5855.
- [18] a) N. Meethong, H.-Y. S. Huang, W. C. Carter, Y.-M. Chiang, *Electrochem. Solid-State Lett.* **2007**, *10*, A134; b) K. Xiang, W. Xing, D. B. Ravnsbaek, L. Hong, M. Tang, Z. Li, K. M. Wiaderek, O. J. Borkiewicz, K. W. Chapman, P. J. Chupas, Y.-M. Chiang, *Nano Lett.* **2017**, *17*, 1696–1702; c) C. K. Christensen, M. A. Karlsen, A. O. Drejer, B. P. Andersen, C. L. Jakobsen, M. Johansen, D. R. Sorensen, I. Kantor, M. R. V. Jorgensen, D. B. Ravnsbaek, *J. Synchrotron Radiat.* **2023**, *30*, 561–570.
- [19] A. K. Padhi, K. S. Nanjundaswamy, J. B. Goodenough, *J. Electrochem. Soc.* **1997**, *144*, 1188–1194.
- [20] a) O. Dolotko, A. Senyshyn, M. J. Mühlbauer, K. Nikolicowski, H. Ehrenberg, *J. Power Sources* **2014**, *255*, 197–203; b) C. D. Quilty, D. C. Bock, S. Yan, K. J. Takeuchi, E. S. Takeuchi, A. C. Marschilok, *J. Phys. Chem. C* **2020**,

- 124, 8119–8128; c) Y. N. Zhou, J. L. Yue, E. Hu, H. Li, L. Gu, K. W. Nam, S. M. Bak, X. Yu, J. Liu, J. Bai, E. Dooryhee, Z. W. Fu, X. Q. Yang, *Adv. Energy Mater.* **2016**, *6*.
- [21] C. K. Christensen, D. B. Ravnsbæk, in *Sodium-Ion Batteries*, Wiley-VCH GmbH, Wiesbaden, Germany, **2022**, pp. 189–213.
- [22] C. Delmas, C. Fouassier, P. Hagenmuller, *Physica B + C* **1980**, *99*, 81–85.
- [23] A. Ø. Drejer, M. S. Pedersen, M. Johansen, D. B. Ravnsbæk, *ACS Appl. Energ. Mater.* **2023**, *6*, 4909–4921.
- [24] a) A. Deb, U. Bergmann, E. J. Cairns, S. P. Cramer, *J. Synchrotron Radiat.* **2004**, *11*, 497–504; b) O. Haas, A. Deb, E. J. Cairns, A. Wokaun, *J. Electrochem. Soc.* **2005**, *152*, A191–A196.

Manuscript received: January 18, 2024
Revised manuscript received: April 23, 2024
Accepted manuscript online: May 14, 2024
Version of record online: June 24, 2024
